Science Advances
AAAS

advances.sciencemag.org/cgi/content/full/6/31/eabb6003/DC1

Supplementary Materials for

Giant, unconventional anomalous Hall effect in the metallic frustrated magnet candidate, KV_3Sb_5

Shuo-Ying Yang, Yaojia Wang, Brenden R. Ortiz, Defa Liu, Jacob Gayles, Elena Derunova, Rafael Gonzalez-Hernandez, Libor Šmejkal, Yulin Chen, Stuart S. P. Parkin, Stephen D. Wilson, Eric S. Toberer, Tyrel McQueen, Mazhar N. Ali*

*Corresponding author. Email: maz@berkeley.edu

Published 31 July 2020, *Sci. Adv.* **6**, eabb6003 (2020)
DOI: 10.1126/sciadv.abb6003

This PDF file includes:

DEVICE FABRICATION AND CHARACTERIZATION

Bulk KV_3Sb_5 crystals were mechanically exfoliated using Scotch tape on Si/SiO_2(275 nm) substrate. Exfoliated flakes were first screened using an optical microscope. The thickness of the selected flakes were then measured using an atomic force microscope (AFM). Figure 1a shows the AFM image of a typical flake of KV_3Sb_5, which has the thickness of $\approx$ 105 nm as shown in the extracted profile in Fig. 1b. Electrical contacts were then patterned by standard electron-beam lithography and Ru/Au (10 nm/ 200 nm) electrodes were deposited using sputtering. Figure 1c shows the optical image of a typical device used in this work.

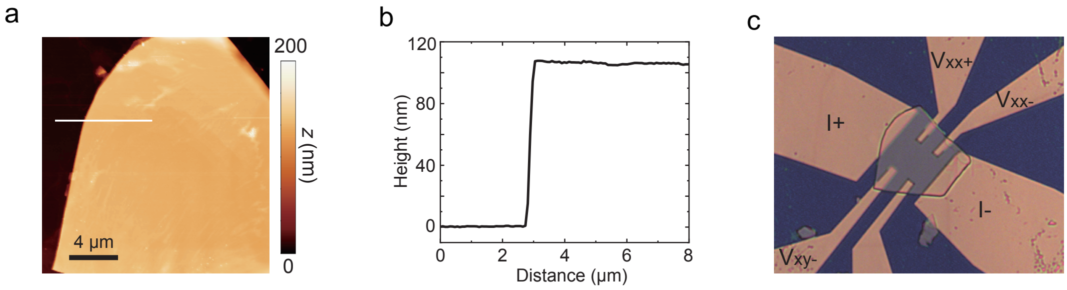

FIG. 1: AFM topography and optical image of a typical device. (a) AFM image of an KV_3Sb_5 exfoliated flake. (b) Extracted height profile of the nanoflake shown in (a). (c) Optical image of a typical device used in this work.

TEMPERATURE AND ANGLE DEPENDENCE OF THE MAGNETORESISTANCE

Temperature dependent magnetoresistance measurements were performed between 1.6 K and 20 K with the field applied in the out-of-plane direction, as shown in Fig. 2. After subtracting a monotonic background (Fig. 2b), the longitudinal ΔR shows a clear damping of SdH amplitude with increasing temperature. The carrier effective mass m^* is extracted by fitting the ΔR as a function of temperature:

$$R_T = \frac{2\pi^2(k_B T/\hbar\omega_c)}{\sinh[2\pi^2(k_B T/\hbar\omega_c)]} \tag{1}$$

where k_B is the Boltzmann constant, $\hbar$ is the Planck constant and ω_c is the cyclotron frequency ($\omega_c = \frac{eB}{m^*}$).

Detailed angle-dependent magnetoresistance measurements were also performed at 2 K with the field applied from the out-of-plane direction to the in-plane direction, as shown in Fig. 2c, in which clear SdH oscillations are observable at different angles. The FFT reveals the angle dependence of orbit frequency as shown in Fig. 2d. The frequency as a function of angle is plotted in the inset, which appears independent of θ when θ is below 20°, and then follows a $1/cos$ above 20°.

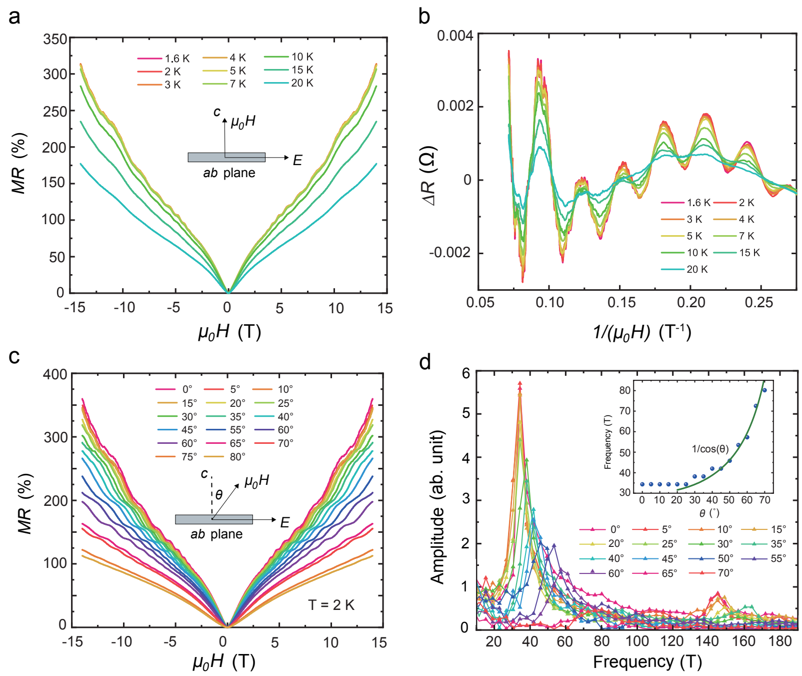

FIG. 2: Temperature and angle dependence of magnetoresistance. (a) Magnetoresistance with field applied out-of-plane measured at various temperatures that are used for the LK fitting in the main text. (b) The temperature dependence of magnetoresistance after subtracting a monotonic background plotted against inverse of field. The oscillation amplitude damps as temperature increases. (c) Angle dependence of magnetoresistance as field is applied from out-of-plane to in-plane at 2 K. The SdH oscillations are observed at different angles. (d) Extracted FFT frequency with field applied at various angles. The inset shows the FFT frequency as a function of angle between the field direction and the out-of-plane direction.

ANGLE DEPENDENCE OF HALL EFFECT MEASUREMENTS

Detailed angle-dependent Hall effect measurements are performed at 2 K with the field applied from the out-of-plane direction to the in-plane direction, as shown in Fig. 4a and 4b. Similar to the magnetoresistance, clear SdH oscillations are observable at different angles. As the field is tilted from out-of-plane to in-plane, the Hall resistivity decreases in magnitude. As it goes past 90°, both the ordinary Hall signal (high field regime) as well as anomalous Hall signal (low field regime) switch sign, signifying that both are true Hall signals.

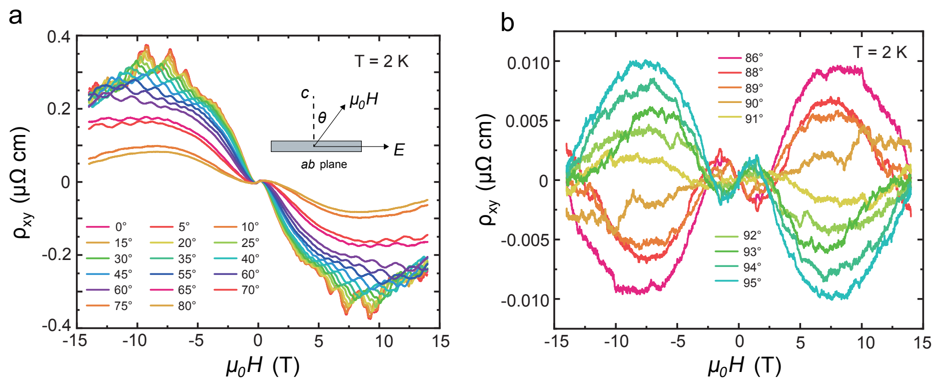

FIG. 3: Angle dependence of the Hall effect measurements. (a) The angle dependence of Hall as the field is applied from out-of-plane to in-plane at 2 K. (b) As the field goes past 90°, the overall Hall response switches sign.

ROBUSTNESS OF ANOMALOUS HALL EFFECT EXTRACTION

There are two nonlinearities in the Hall response of KV_3Sb_5: a low-field, low temperature "S" shape and a high-field, low-temperature nonlinear curve. Through temperature and magnetic field dependence measurement, we find that at high temperature, the high field Hall effect evolves into a linear Hall response while the low field nonlinearity sustains. This enables us to distinguish the origin of nonlinear Hall resistivity at low and high field: the low field nonlinearity comes from the nonspontaneous AHE, and the high field nonlinearity originates from the OHE that evolves from two-band to one-band type with increasing temperature. The zoom-in plot of the Hall resistivity shows that the low field ordinary Hall resistivity is consistently linear in the field range between 1 T and 2 T over the whole temperature range, allowing us to robustly subtract the background OHE in the AHE-relevant region. The angle-dependence measurement is also a supporting evidence that the low-field nonlinearity does not originate from the OHE: OHE should scale linearly with the out-of-plane component of the external magnetic field, which is clearly not the case as shown in Figure 3a in the main text. Furthermore, the intrinsic AHC extracted experimentally matches well with the theoretically calculated AHC. This provides a sanity check and confirms the robustness of the AHE extraction that was not contaminated by an unaccounted OHE contribution.

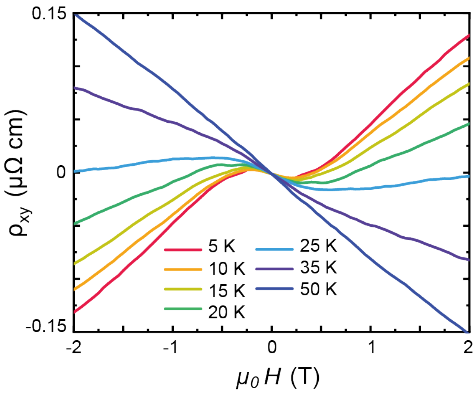

FIG. 4: Zoom-in plot of the Hall resistivity at different temperatures. Zoom-in plot of the Hall resistivity at different temperatures, showing the low field ordinary Hall resistivity is consistently linear in the field range between 1 T and 2 T over the whole temperature range.

AB INITIO ELECTRONIC STRUCTURE AND INTRINSIC HALL CONDUCTIVITY IN KV_3SB_5

KV_3Sb_5 crystal is formed by the Kagome lattice of Vanadium atoms intercalated with a graphite lattice of one of the antimony positions, as shown in Fig. 5a. It crystallizes in the symmorphic space group which is known to host gapped Dirac quasiparticles in the quasi-2D Brillouin zone wedge ΓKMΓ.

The density functional theory (DFT) calculations were performed in the VASP package[52] employing the projector augmented plane wave method[53] and spherically symmetric Dudarev DFT+U[54] is used with U = 2 eV. The energy cut-off of the plane wave basis of 520 eV, the PBE exchange correlation function[55], and the crystal momentum grid $11 \times 11 \times 6$ is chosen. While the Dirac points are gapless in our calculations without SOC, adding the SOC in the calculations generates tiny gaps shown in Fig. 5b (e.g. 10 meV at K point) at the Dirac points since the symmorphic rotational symmetries cannot protect the Dirac crossings[56]. This behavior is exactly analogous to the Dirac semimetal graphene and also other Kagome systems such as Fe_3Sn_2[43], which the ARPES of Fig. 1b establishes. Furthermore, as we highlight by grey shading in the Fig. 5b the system behaves as a semimetal because the states at the Fermi level are comprised from the Dirac quasiparticle set of bands with electron/hole semi-metallic pockets.

The application of magnetism further splits the Dirac quasiparticles, as shown in Fig. 5c. Since the detailed microscopic magnetism is not known[33], for the purpose of our DFT calculations, to determine the possible intrinsic anomalous Hall conductivity component, we used the experimental lattice parameters, Wyckoff positions, and assumed the ferromagnetic moments on Vanadium are along the [0001] axis with electronic correlation U = 2 eV. This value of electronic correlations gives a magnetization consistent to the effective magnetic moment observed in[33]. With constructed maximally localized Wannier function in the Wannier90 code[57], intrinsic anomalous Hall conductivity is calculated by employing the Berry curvature formula[58,59] using the fine-mesh of $320 \times 320 \times 240$ Brillouin zone sampling points. Note that the calculated ground-state magnetic moment (0.25 μB per Vanadium atom) matches well with experimentally determined effective moment observed by Ortiz et al[33] (0.22μB per Vanadium atom). The Berry curvature driven intrinsic AHC calculated from the ferromagnetic assumption represents the upper boundary for the intrinsic AHC observed in the experiment in the samples in the "low conductivity" regime. This intrinsic component is separate from the giant extrinsic AHC we observe.

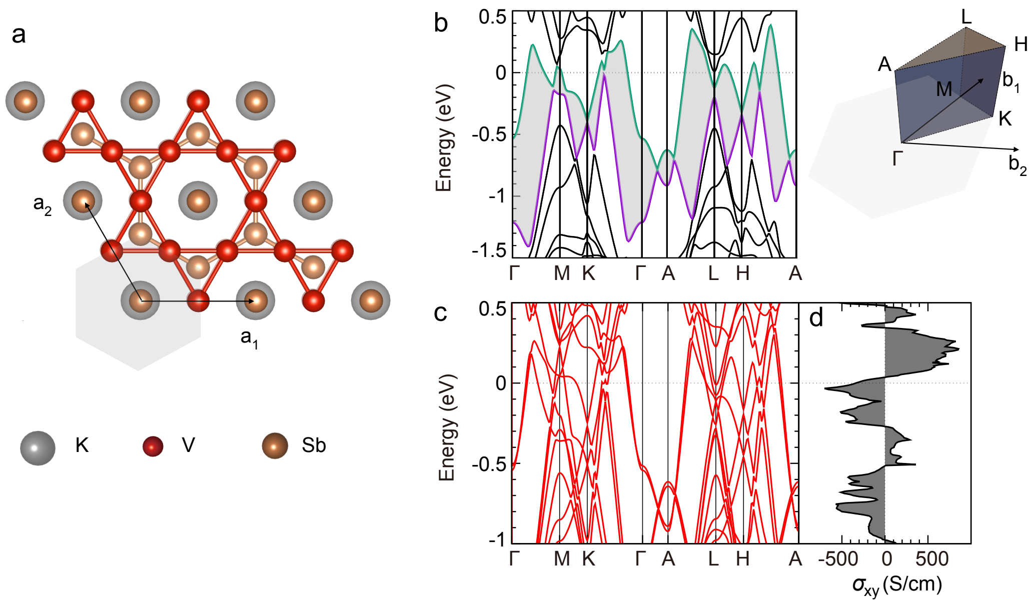

FIG. 5: Ab initio electronic structure and intrinsic Hall conductivity in ferromagnetic KV_3Sb_5. (a) Top view of the crystal with Kagome plane coinciding with the Hall plane. (b) Band structure (Brillouinzone shown to the right) with SOC without ferromagnetism. Green and purple bands comprise the Fermi surface. Grey shaded region denotes the continuous gap illustrating the semimetallic nature of KV_3Sb_5. (c) Band structure calculated in the ferromagnetic state with U = 2 eV and ground-state moments 0.25 μB per Vanadium atom. (d) Energy resolved intrinsic Hall conductivity (x-axis is oriented along the a-crystal axis.)

REFERENCES AND NOTES

1. N. Nagaosa, J. Sinova, S. Onoda, A. H. MacDonald, N. P. Ong, Anomalous Hall effect. *Rev. Mod. Phys.* **82**, 1539 (2010).

2. R. Karplus, J. M. Luttinger, Hall effect in ferromagnetics. *Phys. Rev.* **95**, 1154 (1954).

3. J. Smit, The spontaneous Hall effect in ferromagnetics I. *Physica* **21**, 877–887 (1955).

4. J. Smit, The spontaneous Hall effect in ferromagnetics II. *Physica* **24**, 39–51 (1958).

5. E. M. Pugh, N. Rostoker, Hall effect in ferromagnetic materials. *Rev. Mod. Phys.* **25**, 151 (1953).

6. T. Liang, J. Lin, Q. Gibson, S. Kushwaha, M. Liu, W. Wang, H. Xiong, J. A. Sobota, M. Hashimoto, P. S. Kirchmann, Z.-X. Shen, R. J. Cava, N. P. Ong, Anomalous Hall effect in $ZrTe_5$. *Nat. Phys.* **14**, 451–455 (2018).

7. N. Manyala, Y. Sidis, J. F. DiTusa, G. Aeppli, D. P. Young, Z. Fisk, Large anomalous Hall effect in a silicon-based magnetic semiconductor. *Nat. Mater.* **3**, 255–262 (2004).

8. R. Yu, W. Zhang, H.-J. Zhang, S.-C. Zhang, X. Dai, Z. Fang, Quantized anomalous Hall effect in magnetic topological insulators. *Science* **329**, 61–64 (2010).

9. C.-Z. Chang, J. Zhang, X. Feng, J. Shen, Z. Zhang, M. Guo, K. Li, Y. Ou, P. Wei, L.-L. Wang, Z.-Q. Ji, Y. Feng, S. Ji, X. Chen, J. Jia, X. Dai, Z. Fang, S.-C. Zhang, K. He, Y. Wang, L. Lu, X.-C. Ma, Q.-K. Xue, Experimental observation of the quantum anomalous Hall effect in a magnetic topological insulator. *Science* **340**, 167–170 (2013).

10. C.-X. Liu, S.-C. Zhang, X.-L. Qi, The quantum anomalous Hall effect: Theory and experiment. *Annu. Rev. Condens. Matter Phys.* **7**, 301–321 (2016).

11. C.-Z. Chang, W. Zhao, D. Y. Kim, H. Zhang, B. A. Assaf, D. Heiman, S.-C. Zhang, C. Liu, M. H. W. Chan, J. S. Moodera, High-precision realization of robust quantum anomalous Hall state in a hard ferromagnetic topological insulator. *Nat. Mater.* **14**, 473–477 (2015).

12. A. Bestwick, E. J. Fox, X. Kou, L. Pan, K. L. Wang, D. Goldhaber-Gordon, Precise quantization of the anomalous Hall effect near zero magnetic field. *Phys. Rev. Lett.* **114**, 187201 (2015).

13. G. Sundaram, Q. Niu, Wave-packet dynamics in slowly perturbed crystals: Gradient corrections and Berry-phase effects. *Phys. Rev. B* **59**, 14915 (1999).

14. M. Onoda, N. Nagaosa, Topological nature of anomalous Hall effect in ferromagnets. *J. Phys. Soc. Jpn.* **71**, 19–22 (2002).

15. T. Jungwirth, Q. Niu, A. H. MacDonald, Anomalous Hall effect in ferromagnetic semiconductors. *Phys. Rev. Lett.* **88**, 207208 (2002).

16. Q. Wang, Y. Xu, R. Lou, Z. Liu, M. Li, Y. Huang, D. Shen, H. Weng, S. Wang, H. Lei, Large intrinsic anomalous Hall effect in half-metallic ferromagnet $Co_3Sn_2S_2$ with magnetic Weyl fermions. *Nat. Commun.* **9**, 3681 (2018).

17. K. Manna, C. Felser, J. Gooth, S. N. Guin, T.-H. Kao, J. Kübler, L. Müchler, J. Noky, C. Shekhar, R. Stinshoff, Y. Sun, Topological magnetic Heuslers: Role of symmetry and the Berry phase.

18. S. N. Guin, K. Manna, J. Noky, S. J. Watzman, C. Fu, N. Kumar, W. Schnelle, C. Shekhar, Y. Sun, J. Gooth, C. Felser, Anomalous Nernst effect beyond the magnetization scaling relation in the ferromagnetic Heusler compound Co_2MnGa. *NPG Asia Mater.* **11**, 16 (2019).

19. L. Berger, Side-jump mechanism for the Hall effect of ferromagnets. *Phys. Rev. B* **2**, 4559 (1970).

20. L. Berger, Influence of spin orbit interaction on the transport processes in ferromagnetic nickel alloys, in the presence of a degeneracy of the 3d band. *Physica* **30**, 1141–1159 (1964).

21. P. N. Dheer, Galvanomagnetic effects in iron whiskers. *Phys. Rev.* **156**, 637 (1967).

22. Y. Tian, L. Ye, X. Jin, Proper scaling of the anomalous Hall effect. *Phys. Rev. Lett.* **103**, 087206 (2009).

23. T. Miyasato, N. Abe, T. Fujii, A. Asamitsu, S. Onoda, Y. Onose, N. Nagaosa, Y. Tokura, Crossover behavior of the anomalous Hall effect and anomalous nernst effect in itinerant ferromagnets. *Phys. Rev. Lett.* **99**, 086602 (2007).

24. D. Maryenko, A. S. Mishchenko, M. S. Bahramy, A. Ernst, J. Falson, Y. Kozuka, A. Tsukazaki, N. Nagaosa, M. Kawasaki, Observation of anomalous Hall effect in a non-magnetic two-dimensional electron system. *Nat. Commun.* **8**, 14777 (2017).

25. H. Ishizuka, N. Nagaosa, Theory of giant skew scattering by spin cluster. arXiv preprint arXiv:1906.06501 (2019).

26. G. Tatara, H. Kawamura, Chirality-driven anomalous Hall effect in weak coupling regime. *J. Physical Soc. Japan* **71**, 2613–2616 (2002).

27. H. Kawamura, Anomalous Hall effect as a probe of the chiral order in spin glasses. *Phys. Rev. Lett.* **90**, 047202 (2003).

28. H. Ishizuka, N. Nagaosa, Spin chirality induced skew scattering and anomalous Hall effect in chiral magnets. *Sci. Adv.* **4**, eaap9962 (2018).

29. X.-P. Yao, G. Chen, $Pr_2Ir_2O_7$: When Luttinger semimetal meets Melko-Hertog-Gingras spin ice state. *Phys. Rev. X* **8**, 041039 (2018).

30. H. Okabe, M. Hiraishi, A. Koda, K. M. Kojima, S. Takeshita, I. Yamauchi, Y. Matsushita, Y. Kuramoto, R. Kadono, Metallic spin-liquid-like behavior of LiV_2O_4. *Phys. Rev. B* **99**, 041113(R) (2019).

31. S. Nakatsuji, Y. Machida, Y. Maeno, T. Tayama, T. Sakakibara, J. van Duijn, L. Balicas, J. N. Millican, R. T. Macaluso, J. Y. Chan, Metallic spin-liquid behavior of the geometrically frustrated kondo lattice $Pr_2Ir_2O_7$. *Phys. Rev. Lett.* **96**, 087204 (2006).

32. Y. Shimizu, H. Takeda, M. Tanaka, M. Itoh, S. Niitaka, H. Takagi, An orbital-selective spin liquid in a frustrated heavy fermion spinel LiV_2O_4. *Nat. Commun.* **3**, 981 (2012).

33. B. R. Ortiz, L. C. Gomes, J. R. Morey, M. Winiarski, M. Bordelon, J. S. Mangum, I. W. H. Oswald, J. A. Rodriguez-Rivera, J. R. Neilson, S. D. Wilson, E. Ertekin, T. M. McQueen, E. S. Toberer, New kagome prototype materials: Discovery of KV_3Sb_5, RbV_3Sb_5, and CsV_3SB_5. *Phys. Rev. Mater.* **3**, 094407 (2019).

34. D. Hou, G. Su, Y. Tian, X. Jin, S. A. Yang, Q. Niu, Multivariable scaling for the anomalous Hall effect. *Phys. Rev. Lett.* **114**, 217203 (2015).

35. K. Behnia, L. Balicas, Y. Kopelevich, Signatures of electron fractionalization in ultra-quantum bismuth. *Science* **317**, 1729–1731 (2007).

36. L. Ye, Y. Tian, X. Jin, D. Xiao, Temperature dependence of the intrinsic anomalous Hall effect in nickel. *Phys. Rev. B* **85**, 220403(R) (2012).

37. S. Sangiao, L. Morellon, G. Simon, J. M. De Teresa, J. A. Pardo, J. Arbiol, M. R. Ibarra, Anomalous Hall effect in Fe (001) epitaxial thin films over a wide range in conductivity. *Phys. Rev. B* **79**, 014431 (2009).

38. R. Schad, P. Beliën, G. Verbanck, V. Moshchalkov, Y. Bruynseraede, Analysis of the transport properties of epitaxial Fe and Cr films. *J. Phys. Condens. Matter* **10**, 6643–6650 (1998).

39. S. Iguchi, N. Hanasaki, Y. Tokura, Scaling of anomalous Hall resistivity in $Nd_2 (Mo_{1-x}Nb_x)_2O_7$ with spin chirality. *Phys. Rev. Lett.* **99**, 077202 (2007).

40. S. Nakatsuji, N. Kiyohara, T. Higo, Large anomalous Hall effect in a non-collinear antiferromagnet at room temperature. *Nature* **527**, 212–215 (2015).

41. E. Liu, Y. Sun, N. Kumar, L. Muechler, A. Sun, L. Jiao, S.-Y. Yang, D. Liu, A. Liang, Q. Xu, J. Kroder, V. Süß, H. Borrmann, C. Shekhar, Z. Wang, C. Xi, W. Wang, W. Schnelle, S. Wirth, Y. Chen, S. T. B. Goennenwein, C. Felser, Giant anomalous Hall effect in a ferromagnetic kagome-lattice semimetal. *Nat. Phys.* **14**, 1125–1131 (2018).

42. A. K. Nayak, J. E. Fischer, Y. Sun, B. Yan, J. Karel, A. C. Komarek, C. Shekhar, N. Kumar, W. Schnelle, J. Kübler, C. Felser, S. S. P. Parkin, Large anomalous Hall effect driven by a nonvanishing Berry curvature in the noncolinear antiferromagnet Mn3Ge. *Sci. Adv.* **2**, e1501870 (2016).

43. L. Ye, M. Kang, J. Liu, F. von Cube, C. R. Wicker, T. Suzuki, C. Jozwiak, A. Bostwick, E. Rotenberg, D. C. Bell, L. Fu, R. Comin, J. G. Checkelsky, Massive Dirac fermions in a ferromagnetic kagome metal. *Nature* **555**, 638–642 (2018).

44. H. Yang, Y. Sun, Y. Zhang, W.-J. Shi, S. S. P. Parkin, B. Yan, Topological weyl semimetals in the chiral antiferromagnetic materials Mn_3Ge and Mn_3Sn. *New J. Phys.* **19**, 015008 (2017).

45. Y. Taguchi, Y. Oohara, H. Yoshizawa, N. Nagaosa, Y. Tokura, Spin chirality, Berry phase, and anomalous Hall effect in a frustrated ferromagnet. *Science* **291**, 2573–2576 (2001).

46. T. Liang, Q. Gibson, M. N. Ali, M. Liu, R. J. Cava, N. P. Ong, Ultrahigh mobility and giant magnetoresistance in the Dirac semimetal Cd_3As_2. *Nat. Mater.* **14**, 280–284 (2015).

47. C. Zhang, Z. Ni, J. Zhang, X. Yuan, Y. Liu, Y. Zou, Z. Liao, Y. Du, A. Narayan, H. Zhang, T. Gu, X. Zhu, L. Pi, S. Sanvito, X. Han, J. Zou, Y. Shi, X. Wan, S. Y. Savrasov, F. Xiu, Ultrahigh conductivity in Weyl semimetal NbAs nanobelts. *Nat. Mater.* **18**, 482–488 (2019).

48. L. Wang, I. Meric, P. Y. Huang, Q. Gao, Y. Gao, H. Tran, T. Taniguchi, K. Watanabe, L. M. Campos, D. A. Muller, J. Guo, P. Kim, J. Hone, K. L. Shepard, C. R. Dean, One-dimensional electrical contact to a two-dimensional material. *Science* **342**, 614–617 (2013).

49. J. Jiang, F. Tang, X. C. Pan, H. M. Liu, X. H. Niu, Y. X. Wang, D. F. Xu, H. F. Yang, B. P. Xie, F. Q. Song, P. Dudin, T. K. Kim, M. Hoesch, P. Kumar Das, I. Vobornik, X. G. Wan, D. L. Feng, Signature of strong spin-orbital coupling in the large nonsaturating magnetoresistance material WTe_2. *Phys. Rev. Lett.* **115**, 166601 (2015).

50. P. Blaha, K. Schwarz, P. Sorantin, S. Trickey, Full-potential, linearized augmented plane wave programs for crystalline systems. *Comput. Phys. Commun.* **59**, 399–415 (1990).

51. P. Blaha, Computer code wien2k (vienna university of technology, 2002), improved and updated unix version of the original p. blaha, k. schwarz, p. sorantin, sb rickey. *Comput. Phys. Commun.* **59**, 399 (1990).

52. G. Kresse, J. Furthmuller, Efficient iterative schemes for ab initio total-energy calculations using a plane-wave basis set. *Phys. Rev. B* **54**, 11169–11186 (1996).

53. P. E. Blochl, Projector augmented-wave method. *Phys. Rev. B* **50**, 17953–17979 (1994).

54. S. L. Dudarev, G. A. Botton, S. Y. Savrasov, C. J. Humphreys, A. P. Sutton, Electron-energy-loss spectra and the structural stability of nickel oxide: An lsda + u study. *Phys. Rev. B* **57**, 1505–1509 (1998).

55. J. P. Perdew, K. Burke, M. Ernzerhof, Generalized gradient approximation made simple. *Phys. Rev. Lett.* **77**, 3865–3868 (1996).

56. B.-J. Yang, N. Nagaosa, Classification of stable three-dimensional Dirac semimetals with nontrivial topology. *Nat. Commun.* **5**, 4898 (2014).

57. A. A. Mostofi, J. R. Yates, Y.-S. Lee, I. Souza, D. Vanderbilt, N. Marzari, wannier90: A tool for obtaining maximally-localised wannier functions. *Comput. Phys. Commun.* **178**, 685–699 (2008).

58. J. Zelezny, Y. Zhang, C. Felser, B. Yan, Spin-polarized current in noncollinear antiferromagnets. *Phys. Rev. Lett.* **119**, 187204 (2017).

59. L. Smejkal, R. Gonzalez-Hernandez, T. Jungwirth, J. Sinova, Crystal Hall effect in collinear antiferromagnets. arXiv:1901.00445 (2019).